



A hybrid nonlinear vibration energy harvester



Wei Yang, Shahrzad Towfighian*

State University of New York at Binghamton, Binghamton, NY 13902, United States

ARTICLE INFO

Article history:

Received 16 July 2016

Received in revised form 1 December 2016

Accepted 20 December 2016

Keywords:

Nonlinear vibration

Energy harvesting

Internal resonance

Bi-stability

ABSTRACT

Vibration energy harvesting converts mechanical energy from ambient sources to electricity to power remote sensors. Compared to linear resonators that have poor performance away from their natural frequency, nonlinear vibration energy harvesters perform better because they use vibration energy over a broader spectrum. We present a hybrid nonlinear energy harvester that combines bi-stability with internal resonance to increase the frequency bandwidth. A two-fold increase in the frequency bandwidth can be obtained compared to a bi-stable system with fixed magnets. The harvester consists of a piezoelectric cantilever beam carrying a movable magnet facing a fixed magnet. A spring allows the magnet to move along the beam and it provides an extra stored energy to further increase the amplitude of vibration acting as a mechanical amplifier. An electromechanically coupled mathematical model of the system is presented to obtain the dynamic response of the cantilever beam, the movable magnet and the output voltage. The perturbation method of multiple scales is applied to solve these equations and obtain approximate analytical solutions. The effects of various system parameters on the frequency responses are investigated. The numerical approaches of the long time integration (Runge-Kutta method) and the shooting technique are used to verify the analytical results. The results of this study can be used to improve efficiency in converting wasted mechanical vibration to useful electrical energy by broadening the frequency bandwidth.

© 2016 Elsevier Ltd. All rights reserved.

1. Introduction

The growth of ultra-low-power sensor technologies inspires the use of alternative energies. One of the most ubiquitous sources of energy is ambient mechanical vibration, which can be converted to useful electrical energy. This renewable source of energy can replace batteries, which have short lives and high maintenance costs. Most of the current vibration energy harvesters are linear resonators that have a narrow bandwidth, which causes a significant drop in the output once the excitation frequency differs from the resonant frequency. As ambient vibrations have a wide spectrum at the low-frequency range, that defect defeats attempts to use linear resonators as convenient energy harvesters [1].

Increasing the frequency bandwidth of resonators will increase the efficiency of converting mechanical energy to electricity. To increase the bandwidth, several methods introduced nonlinearities into the energy harvesting system [2] such as using stoppers to realize a spring hardening effect [3–5] and using axial static preload to stiffen or soften the structure [6,7]. Researchers also applied parametric excitation to trigger nonlinearity for energy harvesting. Yildirim et al. [8] recently

* Corresponding author.

E-mail addresses: wyang24@binghamton.edu (W. Yang), stowfigh@binghamton.edu (S. Towfighian).

Nomenclature

D_3	electric displacement
e_{31}	piezoelectric constant
S_1	mechanical strain
ϵ_{33}^s	piezoelectric material permittivity constant
E_z	electric field
T_{1s}	mechanical stress
c_{11}	compliance of piezoelectric
$\lambda(t)$	flux linkage
L_p	length of piezoelectric
b_p	width of piezoelectric
h_p	thickness of piezoelectric
L	length of beam
b	width of beam
h_s	thickness of beam
L	length of entire piezoelectric beam
A	cross sectional area of entire piezoelectric beam
ρ	volume density of entire piezoelectric beam
I	moment of inertia
E	modulus of elasticity
k	stiffness of spring
$w(x, t)$	lateral deflection of the beam
$s(t)$	position of movable magnet measured from the fixed support
$S(t)$	position of movable magnet measured from equilibrium position
s_e	equilibrium position of movable magnet
k_1	normalize first natural frequency of cantilever beam
U_{mag}	magnetic potential energy
y	base excitation
β	slope angle of the beam deflection curve with horizontal line
R	resistance load
$\phi_1(x)$	the first mode shape for cantilever beam
$\alpha(t)$	dynamic response of cantilever beam
F_{magx}	magnetic force tangential to the beam length
F_{magy}	magnetic force normal to the beam length
μ_0	permeability of space
d	distance between the tip of the cantilever and fixed magnet
D	horizontal distance between two magnets
N	magnetization moment of magnet
ω_s	natural frequency of the spring
m	mass of movable magnet
s_0	original length of spring
μ_n	damping terms
$v(t)$	voltage
T_0, T_1	two time scales
ϵ	scaling parameter
P_1, P_2	complex variables
$E(T_1)$	a variable
σ_1, σ_2	small detuning parameters
Ω	frequency of excitation

designed a clamped-clamped beam with a movable central magnet inside a coil. The experiment showed frequency softening and a broader bandwidth close to the primary and principal parametric resonances.

Nonlinearity from bi-stable systems can also broaden the frequency bandwidth. Such systems use two magnets (one stationary and one moving) for piezoelectric energy harvesters [9–11] to create a double-well potential function. Their performance was studied under base vibrations of harmonic [11] and random natures [12–16]. Across various excitation levels, bi-stable systems outperformed linear ones. Bi-stable systems also were employed in electromagnetic generators [17,18]. The magnetic force adds cubic stiffness nonlinearity and makes the oscillator a Duffing type with frequency hardening behavior [17,19–22]. Daqaq [23] investigated the response of such harvesters as a unimodal Duffing-type oscillator exposed to White Gaussian and Colored excitation. Combining piezoelectric and electromagnetic energy harvesting mechanisms, a

hybrid nonlinear system was studied by Karami and Inman [24] who introduced a unified model to predict the system behavior. Zou et al. [25] proposed a compressive-mode wideband vibration energy harvester using a combination of bi-stable and flextensional mechanisms.

Most vibration energy harvesters use a single degree-of-freedom system. However, to increase the frequency bandwidth, several multi-degree-of-freedom approaches have been proposed. Wu et al. [26] reported that a two degrees-of-freedom harvester can achieve two close resonant frequencies with significant power outputs by using two cantilever beams with magnetic tips. Tang et al. [27] proposed a piezoelectric harvester composed of a cantilever with a magnetic tip facing a movable magnet, replacing the fixed magnet in typical bi-stable harvesters. The power output had a large amplitude over a broad bandwidth. Using two orthogonal cantilever beams with magnetic tips, Ando et al. [28] presented a coupled bi-stable system that showed high outputs at low frequencies for bi-directional vibrations. Increasing degrees of freedom by adding multiple coiled cantilever beams nearby a fixed magnet was also investigated by Sari et al. [29] that showed increase of the frequency bandwidth for micro electromagnetic generators.

Internal resonance is another nonlinear phenomenon that can be used to broaden the bandwidth [30]. An internal resonator acts as a mechanical amplifier to pump energy from other regions of the frequency spectrum to the harvesting bandwidth. Amplitude frequency responses of internal resonators bend to two opposite frequency directions causing an increase in the frequency bandwidth for energy harvesting. This advantage of internal resonance recently attracted some researchers. Lan et al. [31] investigated the energy harvesting of a vertical piezoelectric beam with its tip mass under vertical excitations. Static and dynamic instabilities was used to create large amplitudes. Strong internal resonance of the system improved energy conversion efficiency under harmonic and random excitations. Adding a mechanical oscillator to an electromagnetic energy harvester, Chen and Jiang [32] demonstrated that energy harvesting based on internal resonance produces more power compared to a linear system through a numerical and analytical study. Using an L-shaped piezoelectric structure with quadratic nonlinearity, Cao et al. [33] showed exploitation of its two-to-one internal resonance increased significant frequency bandwidth compared to its 2-DOF counterpart. This increase was achieved for excitation frequencies near the first and second linear natural frequencies. In addition to an L-shaped piezoelectric beam, Chen et al. [34] used magnets to improve the performance by increasing the bandwidth of energy harvesting. By changing the distance between two magnets, the harvester can apply internal resonance to broaden bandwidth and increase output. Compared to a traditional nonlinear energy harvester including a cantilever with tip magnet facing fixed magnet, Xiong et al. [35] introduced an auxiliary oscillator that produces internal resonance with the main cantilever. It demonstrated that the nonlinearity of internal resonance increases the operating bandwidth by experiment and simulation.

The contributions of this paper is to combine bi-stability and internal resonance effects to broaden the frequency bandwidth of nonlinear vibration energy harvesting. This is achieved by employing a system that is composed of a cantilever beam with a movable magnet facing a fixed magnet. Bi-stability is introduced by the magnetic interactions, while the movable magnet generates internal resonance. Bi-stability can broaden the frequency bandwidth, but the increase is not substantial. Combining the two effects results in a larger frequency bandwidth that can increase energy conversion efficiency. In our preliminary study [36], we developed a mathematical model for a movable magnet on a cantilever beam. In this paper, we add a piezoelectric strip to the beam for energy harvesting and develop an electromechanical coupled mathematical model of the system. We present an approximate analytical solution and numerical verification.

The content of this article is organized as follows. Section 2 describes a mathematical modeling of the combined resonator followed by the perturbation method of multiple scales in Section 3 to solve for the steady-state frequency response. A linearized piezoelectric coupling was used to simulate the electromechanical performance. The obtained solutions are described in Section 4. The effects of various system parameters on the electromechanical frequency responses are investigated in this section and analytical solutions are verified with the numerical solutions. Section 5 concludes the paper.

2. Mathematical modeling

The vibration energy harvester consists of a piezoelectric cantilever beam with a movable magnet attached to a spring, and another fixed magnet with the arrangement of repulsive magnetic force that is depicted in Fig. 1. The cantilever beam is fully covered by the piezoelectric material as the active transducer. The spring on the beam allows the movable magnet to slide along the beam. The whole structure is attached to a parent host that generates a mechanical vibration in the horizontal plane making the beam vibrate in the same plane. Our goal is to increase the vibration amplitude of the cantilever beam to maximize the piezoelectric voltage output. This goal is achieved using the movable magnet and the working principle is explained in the next subsection.

2.1. Working principle

The initial position of beam and magnets is shown in Fig. 1. The vibration of the base normal to the beam length causes two terminal positions of the beam in the horizontal plane (Fig. 2). At the initial, centered, position of the beam, the tangential component of the magnetic force compresses the spring (Fig. 1). As the beam vibrates away from the center position, the effect of the tangential component wanes while the normal component becomes stronger (Fig. 3a). The reduction in the tangential component makes the spring stretch, reducing the horizontal distance between the magnets. The normal component

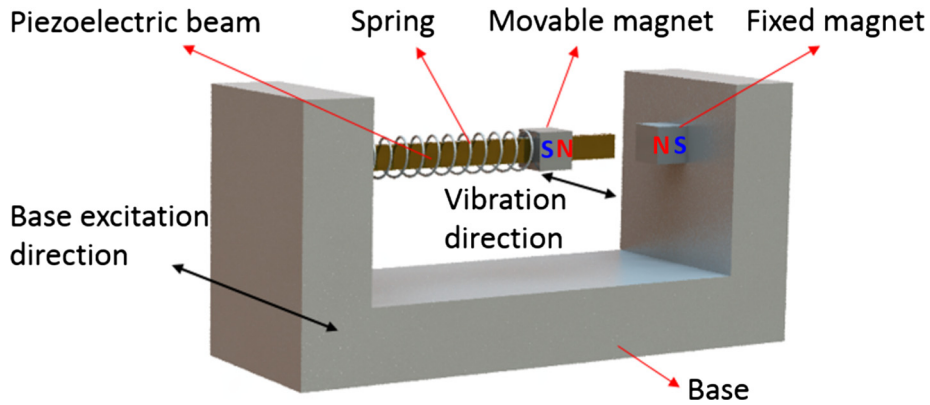
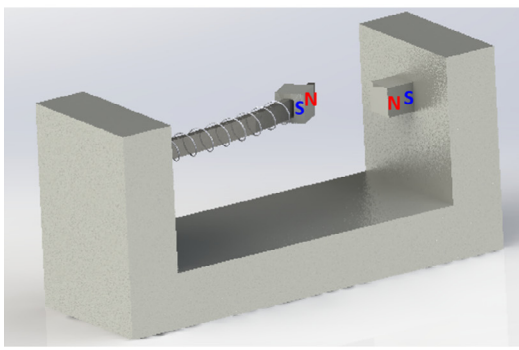
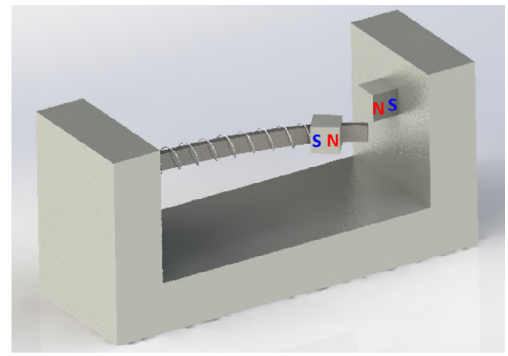


Fig. 1. Nonlinear vibration energy harvesting with internal resonance.



(a)



(b)

Fig. 2. Beam is in two terminal positions.

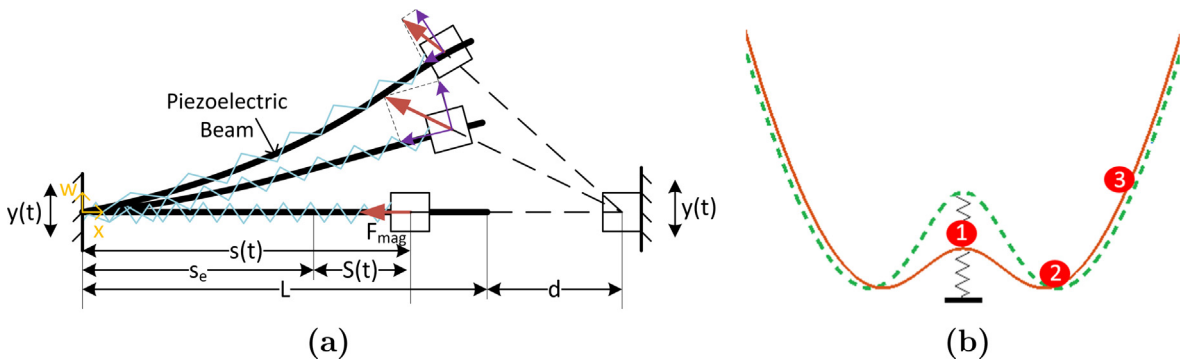


Fig. 3. (a) Schematic of a beam with movable magnet from the top view, (b) variable double well potential function concept.

of the magnetic force increases with this distance reduction, hence bending the beam to its largest displacement. At this terminal position, the restoring force of the beam overcomes the normal magnetic force, the beam vibration reverses, and the spring compresses again. The increase in the beam displacement caused by the increase of the normal magnetic force is unique for this movable magnet configuration. The larger the displacement, the larger the piezoelectric output voltage.

The working principle of the system can also be explained by a variable potential function. The potential energy of the system is a double-well function when the distance between two magnets is below a threshold value, which is shown in Fig. 3b. The motion of the cantilever beam resembles the motion of a heavy ball oscillating in a double well potential function with a flexible bump standing on a spring in the middle. Position 1 shows the ball compressing the spring that represents the beam in its initial position with the solid line potential function. As the ball moves down (as the beam vibrates), the spring

releases the stored energy to create a new potential function (dashed line). The release of spring’s energy helps the ball gain higher velocity at position 2 that pushes the ball to position 3, where the velocity of the ball slows to zero. At position 3, the ball has more potential energy than at the starting position (position 1) because of the added restoring energy of the spring. Then the ball starts moving back. On the way back (from position 2 to position 1), the heavy ball compresses the spring and the potential function will be the solid line again. In this variable potential concept, the key for increasing the height of the ball (equivalent to the beam amplitude) is therefore the added potential energy of the spring. This results in larger electrical energy output.

2.2. Governing equations

To predict the dynamic response and output voltage of the resonator, a mathematical coupled model for the cantilever under the influence of magnets and the piezoelectric strip is derived. The electromechanical model of the piezoelectric behavior is governed by the following constitutive laws relating the mechanical stress to the electric field generated within a layer:

$$\begin{aligned} D_3 &= e_{31}T_{1s} + \epsilon_{33}^s E_z \\ S_1 &= c_{11}T_{1s} + e_{31}E_z \end{aligned} \tag{1}$$

Because of the parallel connection of piezoelectric layers, the electric field can be written in terms of flux linkage $\lambda(t)$ as:

$$E_z = -\frac{\dot{\lambda}(t)}{h_p} \tag{2}$$

The electric energy for one piezoelectric strip is $\frac{1}{2} \int E_z D_3 dv$, where v is the volume of piezoelectric strip. Therefore, the electric energy in the system is [11]

$$2 \times \frac{1}{2} \int E_z D_3 dv = e_{31}b_p(h_p + h_s)\dot{\lambda}(t)w_x(L_p, t) + \epsilon_{33}^s \frac{b_p L_p}{h_p} \dot{\lambda}(t)^2 \tag{3}$$

We write the total energy of the system and use Hamilton’s Principle and variational calculus to derive the equations of motion. Our model builds on the work by Siddiqui et al. [37] who studied the dynamics of a cantilever beam with a moving mass. Here we convert the moving mass to a moving magnet facing a fixed magnet and add the piezoelectric strip

The total kinetic energy of the proposed system is:

$$T = \frac{1}{2} \int_0^L \rho A (\dot{w} + \dot{y})^2 dx + \frac{1}{2} m [\dot{s} \sin \beta + (\dot{w} + \dot{y})]^2 + \frac{1}{2} m (\dot{s} \cos \beta)^2 \tag{4}$$

where β is the slope angle of the beam deflection curve with the horizontal line assuming $\sin \beta = \frac{\partial w}{\partial x}$. Because the width of the beam is aligned along the vertical direction, it has a low moment of inertia about that axis and causes the beam to vibrate only in the horizontal plane. Hence, we can ignore the potential energy from gravity on the movable magnet as it has a negligible effect on the motion of the beam in the horizontal plane. The total potential energy of the system including the electric energy is:

$$V = \frac{1}{2} \int_0^L EI w_{xx}^2 dx + \frac{1}{2} ks^2 + U_{mag} - \theta_e \dot{\lambda}(t)w_x(L_p, t) - \frac{1}{2} c_p \dot{\lambda}(t)^2 \tag{5}$$

where

$$\begin{aligned} \theta_e &= e_{31}b_p(h_p + h_s) \\ c_p &= \epsilon_{33}^s \frac{2b_p L_p}{h_p} \end{aligned}$$

To obtain the governing equations of motion, the extended Hamilton’s Principle,

$$\int_{t_1}^{t_2} [\delta(T - V) + I\delta\lambda] dt = 0$$

is used where t_1 and t_2 are two instants of time in which the variation, δ , is calculated. The variations are determined for kinetic, potential energy, and virtual work of the generalized current (I , rate of change of flux linkage over resistive load R), respectively that yields

$$\begin{aligned} \int \left[\int -\rho A \dot{w} dx \delta w - \int EI w_{xxxx} dx \delta w - EI w_{xx} \delta w_x \Big|_0^L + EI w_{xxx} \delta w \Big|_0^L + m \dot{s} \delta \dot{s} - ks \delta s - \delta U_{mag} + m(\dot{w} + \dot{y}) \delta \dot{w} + m \delta w_x (\dot{w} + \dot{y}) \dot{s} \right. \\ \left. + \theta_e \delta \dot{\lambda}(t) w_x(L_p, t) + c_p \dot{\lambda}(t) \delta \dot{\lambda}(t) - \frac{\dot{\lambda}(t)}{R} \delta \dot{\lambda}(t) \right] dt = 0 \end{aligned} \tag{6}$$

To use Galerkin's decomposition method, the mode shapes need to be determined. The mode shape of the beam with moving mass is different from that of a regular cantilever beam, but it is not significantly different. The difference is certainly not going to be as much as the difference between a cantilever beam mode and that of a beam with an end-mass. So we use a trial function generated from an eigenvalue problem similar to that of our system rather than the actual eigenvalue problem. This will work and produce a reasonably accurate Galerkin expansion, if the trial function and the actual mode shape are close enough [38,39], which is the case here. Hence, the boundary conditions of a cantilever beam is used as

$$\begin{aligned} \frac{\partial^3 w(x,t)}{\partial x^3} &= 0 \text{ at } x = L \\ \frac{\partial^2 w(x,t)}{\partial x^2} &= 0 \text{ at } x = L \\ \frac{\partial w(x,t)}{\partial x} &= 0 \text{ at } x = 0 \\ w(x,t) &= 0 \text{ at } x = 0 \end{aligned} \tag{7}$$

To obtain the ordinary differential equations from the partial differential equations, Galerkin's method with a trial function of the form

$$w(x,t) = \sum_{i=1}^n \phi_i(x)\alpha_i(t)$$

is used, where i indicates the mode shape number. To simplify the derivations, only the first mode shape of the cantilever is used ($i = 1$). The normalized first mode shape is given by

$$\begin{aligned} \phi_1(x) &= \cosh(k_1x) - \cos(k_1x) \\ &\quad - \frac{\cos(k_1) + \cosh(k_1)}{\sin(k_1) + \sinh(k_1)} (\sinh(k_1x) - \sin(k_1x)) \end{aligned}$$

where k_1 is the normalized first natural frequency of cantilever beam. Therefore, we have $\delta w = \phi(x)\alpha(t)$ and $\delta w_x = \phi'(x)\alpha(t)$. Integrating every terms in Eq. (6) by parts and dropping terms for boundary conditions, we obtain

$$\begin{aligned} \int \left[\phi \left(\int -\rho A \ddot{w} - EI w_{xxxx} dx \right) \delta \alpha - m \ddot{s} \delta s - ks \delta s + \phi F_{magy} \delta \alpha + F_{magx} \delta s + m(\dot{w} + \dot{y}) \delta \dot{w} + m w_x \delta(\dot{w} + \dot{y}) \dot{s} + \theta_e \delta w_x(L_p, t) \dot{\lambda}(t) \right. \\ \left. + c_p \dot{\lambda}(t) \delta \dot{\lambda}(t) - \frac{\dot{\lambda}(t)}{R} \delta \lambda(t) \right] dt = 0 \end{aligned} \tag{8}$$

where F_{magx} and F_{magy} are the magnetic force tangential and normal to the beam directions, respectively and

$$\begin{aligned} \int m(\dot{w} + \dot{y}) \delta \dot{w} dt &= \int (-m \phi(\dot{w} + \dot{y}) \delta \alpha - m \phi \dot{w}_x \dot{s} \delta \alpha) dt \\ \int m w_x \delta(\dot{w} + \dot{y}) \dot{s} dt &= \int (m w_x \dot{s} \delta \dot{w} + m w_x (\dot{w} + \dot{y}) \dot{s} \delta s) dt = \int (-m \phi w_x \ddot{s} \delta \alpha - m \phi \dot{w}_x \dot{s} \delta \alpha - m \phi w_{xx} \dot{s}^2 \delta \alpha - m w_x (\ddot{w} + \ddot{y}) \dot{s} \delta s) dt \\ \int \left[\theta_e \delta w_x(L_p, t) \dot{\lambda}(t) + c_p \dot{\lambda}(t) \delta \dot{\lambda}(t) - \frac{\dot{\lambda}(t)}{R} \delta \lambda(t) \right] dt &= \int \left[-\theta_e \dot{w}_x(L_p, t) \delta \lambda(t) + \theta_e \phi'(L_p) \dot{\lambda}(t) \delta \alpha - c_p \ddot{\lambda}(t) \delta \lambda(t) - \frac{\dot{\lambda}(t)}{R} \delta \lambda(t) \right] dt \end{aligned}$$

Then set terms of δs , $\delta \alpha$ and $\delta \lambda(t)$ in Eq. (8) to be zero respectively. Governing equations are obtained by three coupled differential equations as

$$m \ddot{s}(t) + ks(t) + m w_x(x, t) \ddot{w}(x, t) + m w_x(x, t) \ddot{y}(t) - F_{magx} = 0 \tag{9}$$

$$\phi \left(\int_0^L \rho A \ddot{w}(x, t) + EI w_{xxxx}(x, t) dx \right) + m \phi f_a + \phi \int_0^L \rho A dx \ddot{y}(t) + m \phi \ddot{y}(t) - \phi F_{magy} - \theta \dot{\lambda}(t) = 0 \tag{10}$$

$$c_p \ddot{\lambda}(t) + \theta_e \dot{w}_x(L_p, t) + \frac{\dot{\lambda}(t)}{R} = 0 \tag{11}$$

where the coupled acceleration term for the mass is

$$f_a = \ddot{w} + 2\dot{w}_x \dot{s} + w_{xx} \dot{s}^2 + w_x \ddot{s}$$

The first term in the above equation is the acceleration of the beam in the lateral direction, the second term is the Coriolis acceleration, the third is centripetal acceleration and the fourth term is the acceleration of the mass projected in the lateral direction. It should be noted that the above equations are written for small oscillations of the beam around equilibrium

points caused by small excitation levels, which is a reasonable assumption for a vibration energy harvester. Nonlinearity from strain displacement relationships is not included in the governing equations. The magnetic force terms are

$$F_{magx} = \frac{FR}{D^4} \left(1 - \frac{5w^2}{2D^2} \right)$$

$$F_{magy} = \frac{FRw}{D^5} \left(1 - \frac{5w^2}{2D^2} \right)$$

$$FR = \frac{3\mu_0 N^2}{2\pi}$$

$$D = D(t) = L + d - s(t)$$

N is the magnetization moment of magnet. N depends on the physical property and size of magnet. We use a cubic magnet with length of 8 mm. The electromechanical coupling term is

$$\theta = \theta_e \phi'(L)$$

The static equilibrium equation is obtained by setting the time derivative terms equal to zero in Eq. (9):

$$\omega_s^2 (s_0 - s_e) - \frac{FR}{mD^4} = 0 \tag{12}$$

Assuming parameters of the system as listed in Table 1, Eq. (12) is solved to obtain the static equilibrium positions.

In order to obtain the solution to dynamic equations of Eqs. (9)–(11), perturbation method of multiple scales is used. To further simplify the equations, the governing Eqs. (9) and (10) are expanded about their equilibrium points (s_e for the movable magnet and $\alpha = 0$ for the cantilever beam). A Taylor series expansion about the equilibrium position and including terms up to the first derivatives are used for the expansion as

$$\frac{1}{D^n} = \frac{1}{D_e^n} + \frac{nS}{D_e^{n+1}}$$

$$\phi(x)_{x=s(t)} = \phi_e + \phi'_e S$$

where $S = S(t) = s(t) - s_e$ is the dynamic response of the movable magnet about the equilibrium point. $D_e = L + d - s_e$ and $\phi_e = \phi(s_e)$, $\phi'_e = \phi'(s_e)$. The mode shape of the cantilever is expanded using Taylor series around the equilibrium position of the movable magnet and is substituted into governing Eqs. (9) and (10). Dropping static terms yields

$$\ddot{S} + \omega_s^2 S + \phi_e \phi'_e \ddot{\alpha} + \alpha \phi'_e \ddot{y} - \frac{FR}{mD_e^4} \left\{ \frac{4S}{D_e} + \frac{-5}{2} \left(\frac{1}{D_e^2} + \frac{6S}{D_e^3} \right) \alpha^2 (\phi_e + \phi'_e S)^2 \right\} = 0 \tag{13}$$

Table 1
Energy harvester parameters used in simulation.

Parameters	Values
Mass of moving magnet, m	4 g
Magnet size	8 mm × 8 mm × 8 mm
Mass of beam	5.6 g
Length of beam, L	75 mm
Width of beam, b	10 mm
Thickness of beam, h_s	1 mm
Flexural rigidity, EI	0.003 Pa · m ⁴
Damping ratio, μ_1 and μ_2	0.1
Stiffness of the spring, k	250 N/m
Original length of the spring, s_0	57.75 mm
Distance between the beam tip and fixed magnet, d	4.5 mm
Magnetization moment, N	0.53 A m ²
Length of piezoelectric, L_p	75 mm
Width of piezoelectric, b_p	10 mm
Thickness of piezoelectric, h_p	0.254 mm
Permittivity of free space, ϵ_0	8.854 × 10 ⁻¹² F/m
Laminate permittivity, ϵ_{33}	3200 ϵ_0
Coupling coefficient, e_{31}	-20
Equivalent resistive load, R	500 Ω

$$\int_0^L EI\phi''^2 dx + \int_0^L \rho A\phi^2 dx \ddot{\alpha} + (\phi_e + \phi'_e S) \left(\int_0^L \rho A dx + m \right) \ddot{y} + m\phi_e^2 \ddot{\alpha} + 2mS\phi_e \phi'_e \ddot{\alpha} + m\phi\phi' \ddot{S}\alpha + 2m\phi\phi' \dot{S}\dot{\alpha} + m\dot{S}^2 \alpha\phi\phi'' + mS^2 \ddot{\alpha}\phi_e'^2 - \theta\dot{\lambda}(t) - \frac{FR\alpha(\phi_e + \phi'_e S)^2}{D_e^5} \left\{ \left(1 + \frac{5S}{D_e}\right) + \frac{-5}{2} \left(\frac{1}{D_e^2} + \frac{7S}{D_e^3}\right) \alpha^2 (\phi_e + \phi'_e S)^2 \right\} = 0 \quad (14)$$

where ' denotes the derivative with respect to x and

$$\int_0^L EI\phi''^2 dx = \int_0^L EI\phi\phi'''' dx$$

Nonlinear terms with orders higher than quadratic in Eqs. (13) and (14) are dropped. Assuming the contact surface of the beam and the magnet is lubricated, viscous friction between the two is modeled. For the vibration of the beam, air viscous damping is considered. Adding two damping terms μ_n results in

$$\ddot{S} + \omega^2 S + 2\mu_1 \dot{S} + c_1 \ddot{\alpha} + c_2 \alpha^2 + \phi' \alpha \dot{y} = 0 \quad (15)$$

$$\ddot{\alpha} + \omega_1^2 \alpha + 2\mu_2 \dot{\alpha} + 2mc_4 s \ddot{\alpha} + 2mc_4 \dot{S} \dot{\alpha} + mc_4 \ddot{S} \alpha + c_5 s \alpha - \theta \dot{\lambda}(t) + (\phi_e + S\phi'_e) c_y \dot{y} = 0 \quad (16)$$

$$c_p \ddot{\lambda}(t) + \theta \dot{\alpha} + \frac{\dot{\lambda}(t)}{R} = 0 \quad (17)$$

where

$$\omega^2 = \omega_s^2 + c_3 \quad (18)$$

$$c_1 = \phi\phi' \quad (19)$$

$$c_2 = \frac{5FR\phi_e^2}{2mD_e^6} \quad (20)$$

$$c_3 = -\frac{4FR}{mD_e^5} \quad (21)$$

$$\omega_1^2 = \frac{\int_0^L EI\phi''^2 dx}{\int_0^L \rho A\phi^2 dx + m\phi_e^2} - \frac{FR\phi_e^2}{\left(\int_0^L \rho A\phi^2 dx + m\phi_e^2\right)D_e^5} \quad (22)$$

$$c_4 = \frac{\phi_e \phi'_e}{\int_0^L \rho A\phi^2 dx + m\phi_e^2} \quad (23)$$

$$c_5 = -\frac{FR}{\int_0^L \rho A\phi^2 dx + m\phi_e^2} \left(\frac{2\phi_e \phi'_e}{D_e^5} + \frac{5\phi_e^2}{D_e^6} \right) \quad (24)$$

$$c_y = \frac{\int_0^L \rho A dx + m}{\int_0^L \rho A\phi^2 dx + m\phi_e^2} \quad (25)$$

It is noted that the last term in Eqs. (15) and (16) are parametric excitation terms. A parametric counterpart has a zero steady-state response below the initiation threshold amplitude and a small non-zero initial displacement condition is required [40]. The initiation threshold depends on the damping and level of excitation. However, in practice, the ambient vibration available for energy harvesting is very small. Direct excitation always yields a response regardless of the excitation level. Therefore, in our case, direct excitation is investigated while ignoring the parametric excitation condition. The relationship between voltage $v(t)$ and flux linkage $\lambda(t)$ is $v(t) = \dot{\lambda}(t)$. Considering only the direct excitation, the two governing Eqs. (15)–(17) become

$$\ddot{S} + \omega^2 S + 2\mu_1 \dot{S} + c_1 \ddot{\alpha} + c_2 \alpha^2 = 0 \quad (26)$$

$$\ddot{\alpha} + \omega_1^2 \alpha + 2\mu_2 \dot{\alpha} + 2mc_4 s \ddot{\alpha} + 2mc_4 \dot{S} \dot{\alpha} + mc_4 \ddot{S} \alpha + c_5 s \alpha - \theta v(t) = F \cos(\Omega t + \tau) \quad (27)$$

$$c_p v(\dot{t}) + \frac{v(t)}{R} + \theta \dot{\alpha} = 0 \quad (28)$$

where $F \cos(\Omega t + \tau) = -\phi_e c_y \ddot{y}$.

3. Perturbation method of multiple scales

The method of multiple scales is used to obtain an analytical solution to the governing equations and to study the quantitative behavior of the system under various parameters. Two time scales T_0 (fast) and T_1 (slow) are used:

$$T_0 = t$$

$$T_1 = \varepsilon t$$

where ε is a scaling parameter. Let $F = \varepsilon f$, the governing equations become

$$\ddot{S} + \omega^2 S + \varepsilon(2\mu_1 \dot{S} + c_1 \ddot{\alpha} + c_2 \alpha^2) = 0 \quad (29)$$

$$\ddot{\alpha} + \omega_1^2 \alpha + \varepsilon(2\mu_2 \dot{\alpha} + 2mc_4 \dot{S} \ddot{\alpha} + 2mc_4 \dot{S} \dot{\alpha} + mc_4 \ddot{S} \alpha + c_5 S \alpha - \theta v(t)) = \varepsilon f \cos(\Omega t + \tau) \quad (30)$$

$$c_p \dot{v}(t) + \frac{v(t)}{R} + \theta \dot{\alpha} = 0 \quad (31)$$

The next step is to assume an asymptotic series solution for $S(t)$, $\alpha(t)$ and $v(t)$. In this case, a two term expansion is assumed as:

$$S(t) = S_1(T_0, T_1) + \varepsilon S_2(T_0, T_1)$$

$$\alpha(t) = u_1(T_0, T_1) + \varepsilon u_2(T_0, T_1)$$

$$v(t) = v_1(T_0, T_1) + \varepsilon v_2(T_0, T_1) \quad (32)$$

Dropping second and higher order terms, time derivatives are written as

$$\frac{\partial}{\partial t} = \frac{\partial}{\partial T_0} + \varepsilon \frac{\partial}{\partial T_1}$$

$$\frac{\partial^2}{\partial t^2} = \frac{\partial^2}{\partial T_0^2} + 2\varepsilon \frac{\partial^2}{\partial T_0 \partial T_1}$$

Substituting the asymptotic series solution into the time derivatives gives

$$\dot{S} = \frac{\partial S_1}{\partial T_0} + \varepsilon \frac{\partial S_2}{\partial T_0} + \varepsilon \frac{\partial S_1}{\partial T_1} + \varepsilon^2 \frac{\partial S_2}{\partial T_1}$$

$$\ddot{S} = \frac{\partial^2 S_1}{\partial T_0^2} + \varepsilon \frac{\partial^2 S_2}{\partial T_0^2} + 2\varepsilon \frac{\partial^2 S_1}{\partial T_0 \partial T_1} + 2\varepsilon^2 \frac{\partial^2 S_2}{\partial T_0 \partial T_1}$$

$$\dot{\alpha} = \frac{\partial u_1}{\partial T_0} + \varepsilon \frac{\partial u_2}{\partial T_0} + \varepsilon \frac{\partial u_1}{\partial T_1} + \varepsilon^2 \frac{\partial u_2}{\partial T_1}$$

$$\ddot{\alpha} = \frac{\partial^2 u_1}{\partial T_0^2} + \varepsilon \frac{\partial^2 u_2}{\partial T_0^2} + 2\varepsilon \frac{\partial^2 u_1}{\partial T_0 \partial T_1} + 2\varepsilon^2 \frac{\partial^2 u_2}{\partial T_0 \partial T_1}$$

$$\dot{v} = \frac{\partial v_1}{\partial T_0} + \varepsilon \frac{\partial v_2}{\partial T_0} + \varepsilon \frac{\partial v_1}{\partial T_1} + \varepsilon^2 \frac{\partial v_2}{\partial T_1}$$

Plugging the above equations into Eqs. (29)–(31), and equating the coefficient of ε^0 and ε^1 to zero, obtains ε^0 order:

$$\frac{\partial^2 S_1}{\partial T_0^2} + \omega^2 S_1 = 0 \quad (33)$$

$$\frac{\partial^2 u_1}{\partial T_0^2} + \omega_1^2 u_1 = 0 \quad (34)$$

$$c_p \frac{\partial v_1}{\partial T_0} + \frac{v_1}{R} = -\theta \frac{\partial u_1}{\partial T_0} \quad (35)$$

ε^1 order:

$$\frac{\partial^2 S_2}{\partial T_0^2} + \omega^2 S_2 = -2\mu_1 \frac{\partial S_1}{\partial T_0} - 2 \frac{\partial^2 S_1}{\partial T_0 \partial T_1} - c_1 \frac{\partial^2 u_1}{\partial T_0^2} u_1 - c_2 u_1^2 \quad (36)$$

$$\begin{aligned} \frac{\partial^2 u_2}{\partial T_0^2} + \omega_1^2 u_2 &= -2\mu_2 \frac{\partial u_1}{\partial T_0} - 2 \frac{\partial^2 u_1}{\partial T_0 \partial T_1} - 2mc_4 \frac{\partial^2 u_1}{\partial T_0^2} S_1 \\ &- 2mc_4 \frac{\partial S_1}{\partial T_0} \frac{\partial u_1}{\partial T_0} - mc_4 \frac{\partial^2 S_1}{\partial T_0^2} u_1 \\ &- c_5 S_1 u_1 + f \cos(\Omega T_0 + \tau) + \theta v_1 \end{aligned} \quad (37)$$

$$c_p \frac{\partial v_2}{\partial T_0} + \frac{v_2}{R} = -c_p \frac{\partial v_1}{\partial T_1} - \theta \left(\frac{\partial u_2}{\partial T_0} + \frac{\partial u_1}{\partial T_0} \right) \quad (38)$$

The solutions of Eqs. (33)–(35) are given by

$$S_1 = P_1(T_1) e^{i\omega T_0} + \bar{P}_1(T_1) e^{-i\omega T_0} \quad (39)$$

$$u_1 = P_2(T_1) e^{i\omega_1 T_0} + \bar{P}_2(T_1) e^{-i\omega_1 T_0} \quad (40)$$

$$v_1 = \frac{-i\omega_1 \theta P_2 e^{i\omega_1 T_0}}{\frac{1}{R} + i\omega_1 c_p} + \frac{i\omega_1 \theta \bar{P}_2 e^{-i\omega_1 T_0}}{\frac{1}{R} - i\omega_1 c_p} + E(T_1) e^{\frac{T_0}{R c_p}} \quad (41)$$

where P_1 and P_2 are complex variables and $E(T_1)$ is a variable. The overbars denote the complex conjugates. Substituting Eqs. (39)–(41) into the right hand sides of Eqs. (36) and (37) results in

$$\begin{aligned} rhs(36) &= -2\mu_1 i\omega P_1 e^{i\omega T_0} + 2\mu_1 i\omega \bar{P}_1 e^{-i\omega T_0} \\ &- 2i\omega \frac{\partial P_1}{\partial T_1} e^{-i\omega T_0} + 2i\omega \frac{\partial \bar{P}_1}{\partial T_1} e^{-i\omega T_0} + (c_1 \omega_1^2 P_2 e^{i\omega_1 T_0} \\ &+ c_1 \omega_1^2 \bar{P}_2 e^{-i\omega_1 T_0}) (P_2 e^{i\omega_1 T_0} + \bar{P}_2 e^{-i\omega_1 T_0}) \\ &- c_2 P_2^2 e^{2i\omega_1 T_0} - 2c_2 P_2 \bar{P}_2 - c_2 \bar{P}_2^2 e^{-2i\omega_1 T_0} \end{aligned} \quad (42)$$

$$\begin{aligned} rhs(37) &= -2\mu_2 i\omega_1 P_2 e^{i\omega_1 T_0} + 2\mu_2 i\omega_1 \bar{P}_2 e^{-i\omega_1 T_0} \\ &- 2i\omega_1 \frac{\partial P_2}{\partial T_1} e^{i\omega_1 T_0} + 2i\omega_1 \frac{\partial \bar{P}_2}{\partial T_1} e^{-i\omega_1 T_0} \\ &+ mc_4 (2\omega_1^2 + \omega^2 + 2\omega\omega_1) P_1 P_2 e^{i(\omega_1 + \omega) T_0} \\ &+ mc_4 (2\omega_1^2 + \omega^2 - 2\omega\omega_1) \bar{P}_1 \bar{P}_2 e^{i(\omega_1 - \omega) T_0} \\ &+ mc_4 (2\omega_1^2 + \omega^2 + 2\omega\omega_1) \bar{P}_1 \bar{P}_2 e^{-i(\omega_1 + \omega) T_0} \\ &+ mc_4 (2\omega_1^2 + \omega^2 - 2\omega\omega_1) P_1 \bar{P}_2 e^{-i(\omega_1 - \omega) T_0} \\ &- c_5 (P_1 e^{i\omega T_0} + \bar{P}_1 e^{-i\omega T_0}) (P_2 e^{i\omega_1 T_0} + \bar{P}_2 e^{-i\omega_1 T_0}) \\ &+ \frac{1}{2} e^{i(\Omega T_0 + \tau)} + \frac{1}{2} e^{-i(\Omega T_0 + \tau)} \\ &+ \theta \left(\frac{-i\omega_1 \theta P_2 e^{i\omega_1 T_0}}{\frac{1}{R} + i\omega_1 c_p} + \frac{i\omega_1 \theta \bar{P}_2 e^{-i\omega_1 T_0}}{\frac{1}{R} - i\omega_1 c_p} + E(T_1) e^{\frac{T_0}{R c_p}} \right) \end{aligned} \quad (43)$$

To eliminate the secular terms, the coefficients of $e^{i\omega T_0}$ and $e^{i\omega_1 T_0}$ in Eqs. (42) and (43) are set to zero. The linear solution is not significant because under these conditions the coupling between the movable magnet and the cantilever beam is very weak. To study the solution for the coupled motion, we investigate the internal resonance case, assuming

$$\omega = 2\omega_1 + \varepsilon\sigma_2 \quad (44)$$

where σ_2 is small detuning parameters. When σ_2 is zero, we have internal resonance of 1:2 ratio (the ratio of the first frequency of the system to the frequency of the moving magnet). For the frequency of excitation, Ω , there are several cases. We consider the case when Ω is near to ω_1 :

$$\Omega = \omega_1 + \varepsilon\sigma_1 \quad (45)$$

where σ_1 is small detuning parameters. Applying the internal resonance relationship (44) and the condition (45), the elimination of secular terms no longer gives a linear solution. We have more nonlinear terms as

$$-2\mu_1 i\omega P_1 - 2i\omega \frac{\partial P_1}{\partial T_1} + c_1 P_2^2 \omega_1^2 e^{-i\sigma_2 T_1} - c_2 P_2^2 e^{-i\sigma_2 T_1} = 0 \tag{46}$$

$$-2\mu_2 i\omega P_2 - 2i\omega_1 \frac{\partial P_2}{\partial T_1} + \frac{1}{2} f e^{i(\sigma_1 T_1 + \tau)} - i \frac{\omega_1 P_2 \theta^2}{\frac{1}{R} + i\omega_1 c_p} + (2mc_4 \omega_1^2 + mc_4 \omega^2 - 2mc_4 \omega \omega_1 - c_5) P_1 \bar{P}_2 e^{i\sigma_2 T_1} = 0 \tag{47}$$

The complex variable P_1 and P_2 are described in polar form as

$$P_1(T_1) = \frac{1}{2} p_1(T_1) e^{i\phi_1(T_1)}$$

$$P_2(T_1) = \frac{1}{2} p_2(T_1) e^{i\phi_2(T_1)}$$

Setting the real and imaginary parts of Eqs. (46) and (47) to zero respectively yields

$$\frac{\partial p_1}{\partial T_1} = -\mu_1 p_1 + \frac{a_{11}}{4\omega} p_2^2 \sin \gamma_1 \tag{48}$$

$$p_1 \frac{\partial \phi_1}{\partial T_1} = -\frac{a_{11}}{4\omega} p_2^2 \cos \gamma_1 \tag{49}$$

$$\frac{\partial p_2}{\partial T_1} = -\mu_2 p_2 - \frac{a_{22}}{4\omega_1} p_1 p_2 \sin \gamma_1 + \frac{f}{2\omega_1} \sin \gamma_2 + E_1 p_2 \tag{50}$$

$$p_2 \frac{\partial \phi_2}{\partial T_1} = -\frac{a_{22}}{4\omega_1} p_1 p_2 \cos \gamma_1 - \frac{f}{2\omega_1} \cos \gamma_2 + E_2 p_2 \tag{51}$$

where

$$a_{11} = c_1 \omega_1^2 - c_2$$

$$a_{22} = 2mc_4 \omega_1^2 - 2mc_4 \omega \omega_1 + mc_4 \omega^2 - c_5$$

$$\gamma_1 = 2\phi_2 - \phi_1 - \sigma_2 T_1$$

$$\gamma_2 = \sigma_1 T_1 + \tau - \phi_2$$

$$E_1 = -\frac{\frac{\theta^2}{2R}}{\frac{1}{R^2} + \omega_1^2 c_p^2}$$

$$E_2 = \frac{\frac{\theta^2 \omega_1 c_p}{2}}{\frac{1}{R^2} + \omega_1^2 c_p^2}$$

In Eqs. (48)–(51), p_1 and p_2 are modal amplitudes and ϕ_1 and ϕ_2 are corresponding phases. For the steady-state response, we set $\frac{\partial p_1}{\partial T_1} = \frac{\partial p_2}{\partial T_1} = \frac{\partial \phi_1}{\partial T_1} = \frac{\partial \phi_2}{\partial T_1} = 0$ to obtain

$$\begin{aligned} & [a_{22}^2 \omega \sqrt{\mu_1^2 + (2\sigma_1 - \sigma_2)^2} p_1^3 \\ & + [8a_{22} \omega \omega_1 (\mu_1 (\mu_2 - E_1) - (\sigma_1 - E_2) (2\sigma_1 - \sigma_2))] p_1^2 \\ & + [16\omega \omega_1^2 ((\mu_2 - E_1)^2 + (\sigma_1 - E_2)^2) \sqrt{\mu_1^2 + (2\sigma_1 - \sigma_2)^2}] p_1 \\ & - a_{11} f^2 = 0 \end{aligned} \tag{52}$$

$$p_2^2 = \left[\frac{4\omega}{a_{11}} \sqrt{\mu_1^2 + (2\sigma_1 - \sigma_2)^2} \right] p_1 \tag{53}$$

Solving Eqs. (52) and (53) gives the amplitude frequency response. The amplitude of output voltage is given by

$$v = \frac{\omega_1 \theta}{\sqrt{\frac{1}{R^2} + \omega_1^2 c_p^2}} p_2 \tag{54}$$

The stability of the steady-state response can be determined by examining the eigenvalues. If all the eigenvalues of a Jacobian matrix have negative real parts, the corresponding steady state response is stable. If not, the corresponding steady-state response is unstable.

4. Results and discussions

4.1. Simulation results

The response of the energy harvester with the parameters listed in Table 1, is obtained by solving Eqs. (52)–(54). The parameters are chosen to have symmetric internal resonance of 1:2 at $\omega_1 = 16$ Hz and $\omega = 32$ Hz (detuning parameter $\sigma_2 = 0$ in Eq. (44)). The default value of base excitation is set to 1 g. The corresponding frequency response is shown in Fig. 4a and the output voltage frequency response is shown in Fig. 4b. Solid lines represent the stable solution and dashed line represent the unstable solution. There are two branches that are tilted to two opposite directions leading to a broad bandwidth frequency response with a jumping phenomenon observed from varying the frequency of excitation, Ω . The new structure applying internal resonance shows that the frequency bandwidth is two times larger than the original non-linear system using fixed magnets that has only a branch tilted to one direction. The response of the beam correlates to the voltage production of a piezoelectric strip as shown in Fig. 4b. As it can be deduced from these figures, there is a region near the central frequency where the solution is unstable.

Fig. 5 depicts the vibration amplitudes of the beam and movable magnet as functions of the excitation level for different detuning parameters σ_1 (in Eqs. (45)) respectively. A smaller σ_1 means the system works near the resonant frequency. On the contrary, a large value of σ_1 indicates that the system works far from the resonant frequency. Solid lines represent the stable response and dashed lines represent the unstable response. There are two regimes for single and multiple solutions depending on the excitation level. In the multiple solution region, two solutions are stable and one is unstable based on the sign of the eigenvalues. In this region, the response at higher or lower stable branches depends on the initial condition of the system. In the single solution region, regardless of the initial conditions, there is only one solution.

4.2. Parametric study

This section studies the effects on energy harvesting by varying system parameters. Because the beam, but not the movable magnet, response affects the output voltage, for the rest of analysis, only the beam response and output voltage are illustrated. The displacement and voltage frequency responses are depicted in Fig. 6 for different levels of base excitation. They reveal the effect of the external excitation amplitude on the frequency response curves. The response amplitude and frequency bandwidth increase with the excitation level, but it does not affect the tilting of the frequency response unlike bistable resonators. It is observed that the unstable frequency range in the middle increases with the excitation amplitude.

The displacement and output voltage frequency responses for different stiffness values of spring k are plotted in Fig. 7. The value of spring stiffness 250 N/m results in symmetric internal resonance ($\sigma_2 = 0$ in Eqs. (44)). Results show that as k decreases below 250 N/m, the central frequency of the frequency response shifts to the left, $\sigma_2 < 0$ or $\omega < 2\omega_1$. Furthermore, the peak of right branch is larger than the left peak and will have a larger bandwidth on the right side of the central frequency. On the contrary, when k increases beyond 250 N/m, the curve shifts to the right, $\sigma_2 > 0$ or $\omega > 2\omega_1$. In this case, the left branch outperforms the right branch. The stiffness of the spring breaks symmetry and changes the position of the

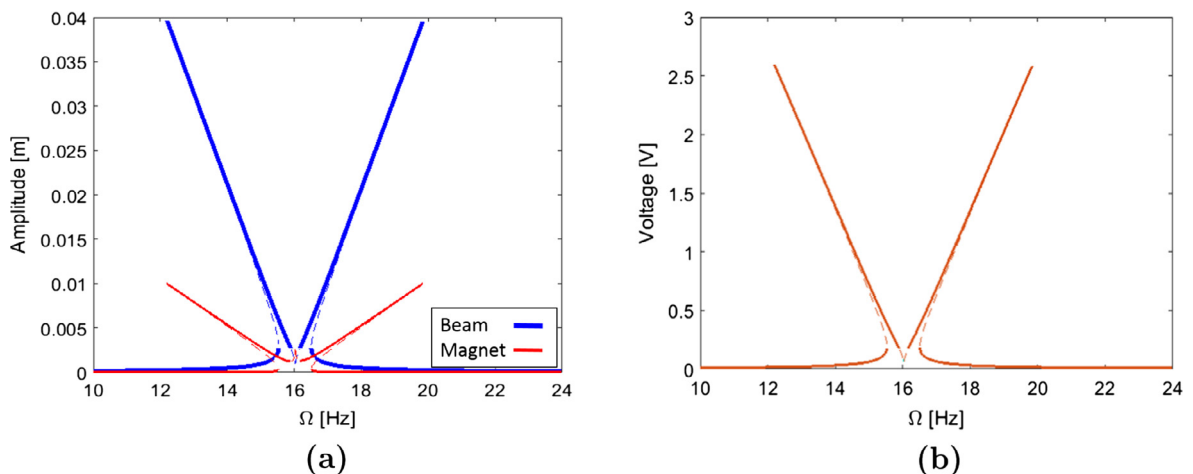


Fig. 4. (a) Frequency response for the beam and moving magnet, (b) output voltage frequency response.

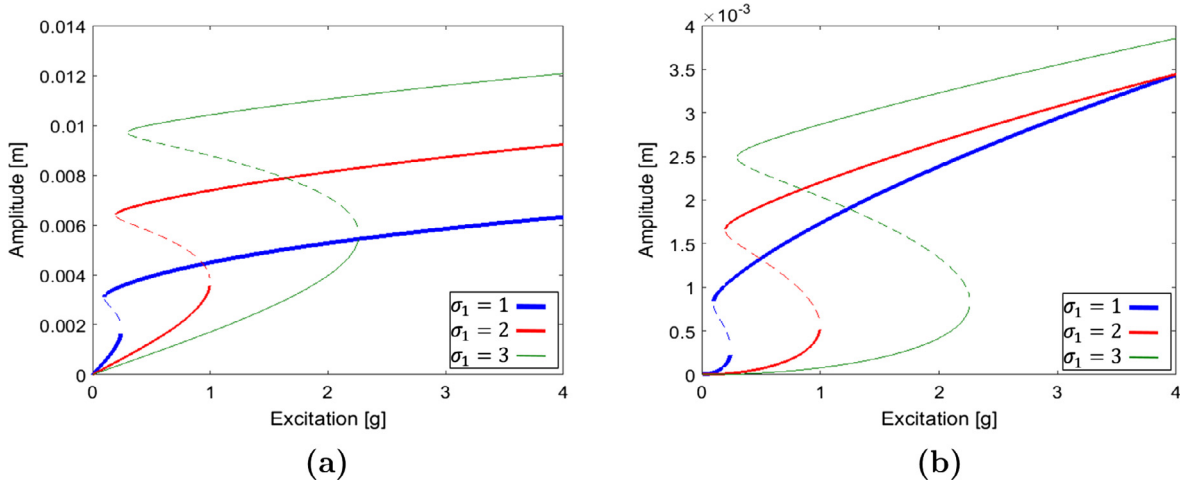


Fig. 5. (a) Beam vibration amplitudes versus excitation level, (b) moving magnet vibration amplitudes versus excitation level.

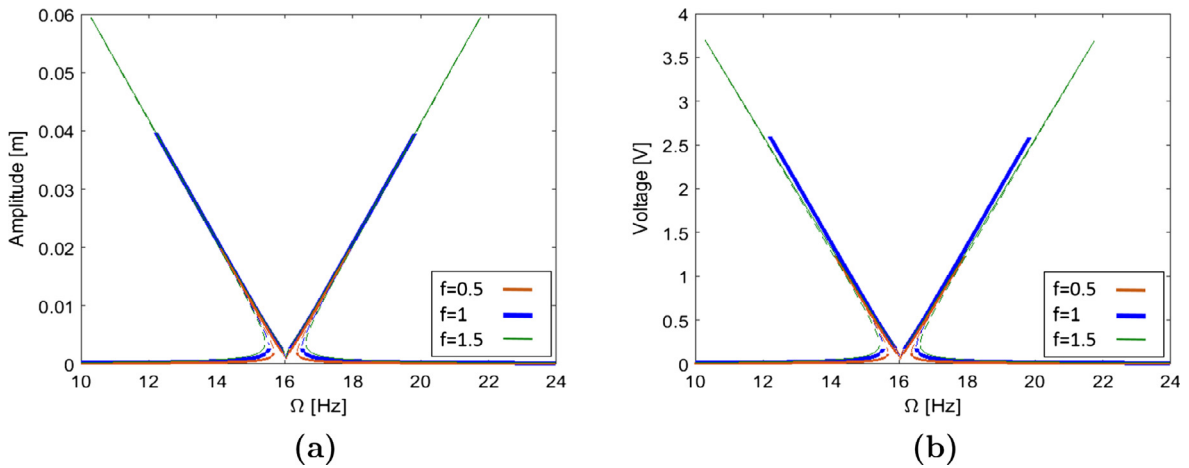


Fig. 6. (a) Frequency response for different excitation levels $f(g)$, (b) Output voltage for different excitation levels $f(g)$.

central frequency with different performances on two branches. Once the symmetry is broken in the frequency response, the frequency bandwidth decreases from 2.3 Hz to 1.6 Hz.

The initial distance between the beam tip and the fixed magnet, d , also affects the frequency responses as shown in Fig. 8. Results show that when d decreases, a broader bandwidth response is obtained with a shift of the central frequency to the left compared to original curve. The bandwidth increases from 2.3 Hz to 2.9 Hz when the distance d decreases from 4.5 mm to 2.5 mm. At smaller d values, the magnetic force is larger making a stronger bi-stability effect that causes larger tilting in the frequency response and output voltage while maintaining a large amplitude in the response.

The magnetization moment effect on the frequency responses is depicted in Fig. 9. The effect is analogous to changing d . In both cases, as the magnetic force strengthens, more tilting occurs in the frequency response. The stronger nonlinear effect on the system creates a broader bandwidth frequency spectrum. We also observe that increasing magnetization moment shifts the central frequency to the left.

4.3. Numerical validations

In order to verify the approximated analytical solutions, two numerical methods are employed to solve Eqs. (26)–(28). The first method is the long time integration (Runge-Kutta method) and the second one is the shooting method [41]. A set of parameters used for making this comparison is listed in the Table 1. The shooting method is a useful way to record periodic solutions of a nonlinear system, and it is computationally more time efficient than the Runge-Kutta method. The procedure of shooting is explained as follows. We let $x_1 = S, x_2 = \dot{S}, x_3 = \alpha, x_4 = \dot{\alpha}$ and $x_5 = \nu(t)$. Then, we set $x_2 = \dot{S}$ and $x_4 = \dot{\alpha}$, which yields

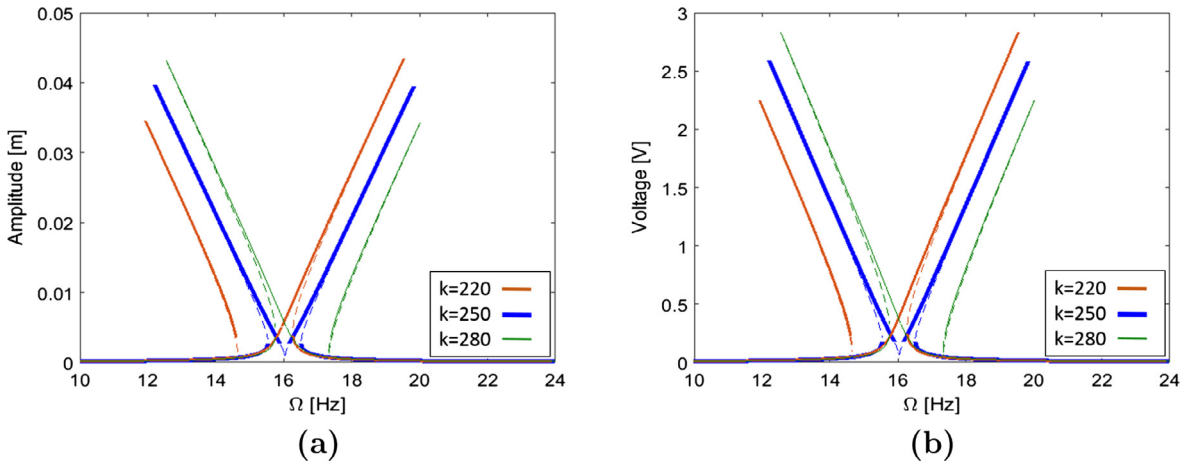


Fig. 7. (a) Frequency response for different excitation levels k (N/m), (b) output voltage for different excitation levels k (N/m).

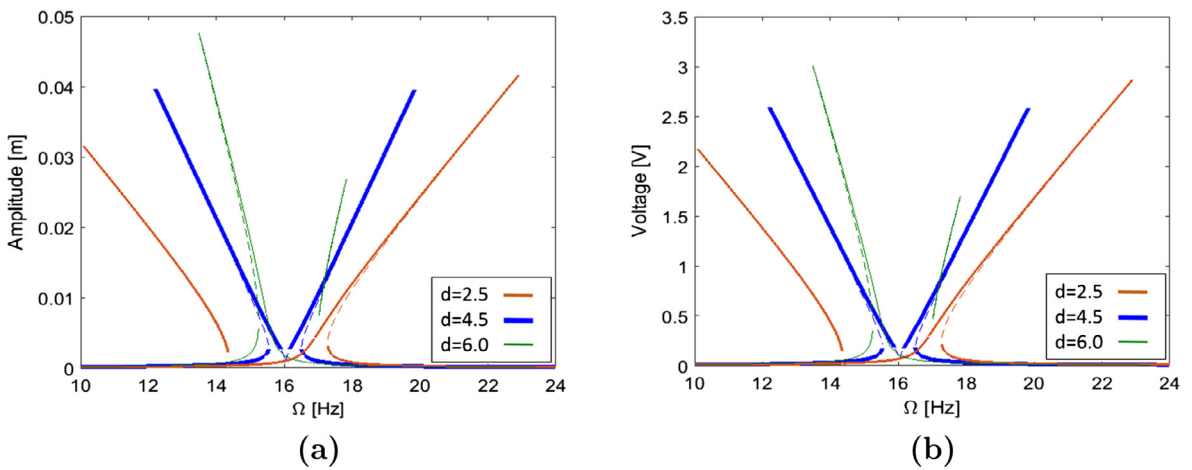


Fig. 8. (a) Frequency response for different distance d (mm), (b) output voltage for different distance d (mm).

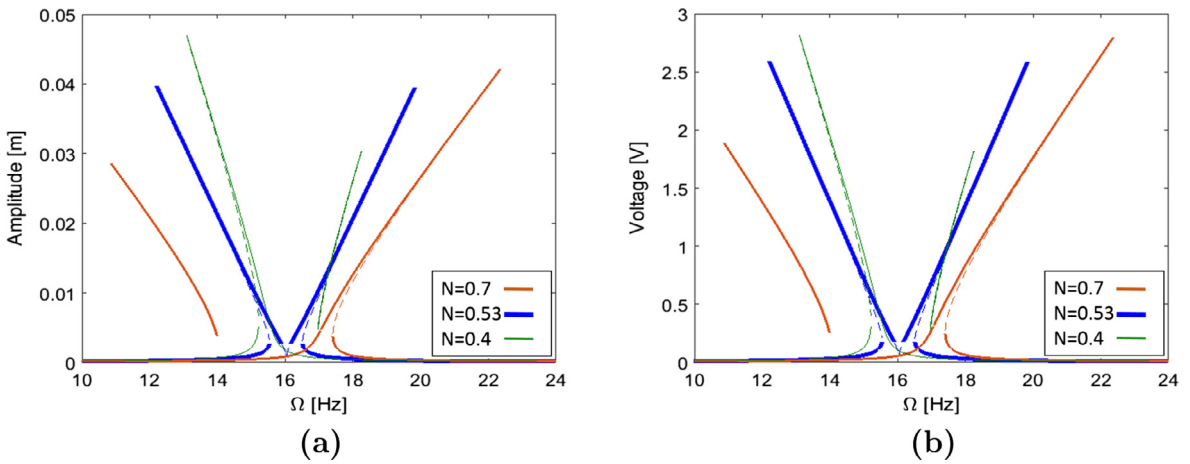


Fig. 9. (a) Frequency response for different magnetization moment N ($A\ m^2$), (b) output voltage for different magnetization moment N ($A\ m^2$).

$$\dot{x}_1 = x_2 \tag{55}$$

$$\dot{x}_2 = -\omega^2 x_1 - 2\mu_1 x_2 - c_1 \dot{x}_4 x_3 - c_2 x_3^2 \tag{56}$$

$$\dot{x}_3 = x_4 \tag{57}$$

$$\dot{x}_4 = -\omega_1^2 x_3 - 2\mu_2 x_4 - 2mc_4 x_1 \dot{x}_4 - 2mc_4 x_2 x_4 - mc_4 \dot{x}_2 x_3 - c_5 x_1 x_3 + \theta x_5 + f \cos \Omega t \tag{58}$$

$$\dot{x}_5 = \left(-\frac{x_5}{R} - \theta x_4 \right) / c_p \tag{59}$$

To proceed with the shooting technique, for convenience, we define the following variables:

$$\begin{aligned} \frac{\partial x_1}{\partial \eta_1} = x_6, \quad \frac{\partial x_1}{\partial \eta_2} = x_7, \quad \frac{\partial x_1}{\partial \eta_3} = x_8, \quad \frac{\partial x_1}{\partial \eta_4} = x_9, \quad \frac{\partial x_1}{\partial \eta_5} = x_{10}, \\ \frac{\partial x_2}{\partial \eta_1} = x_{11}, \quad \frac{\partial x_2}{\partial \eta_2} = x_{12}, \quad \frac{\partial x_2}{\partial \eta_3} = x_{13}, \quad \frac{\partial x_2}{\partial \eta_4} = x_{14}, \quad \frac{\partial x_2}{\partial \eta_5} = x_{15}, \\ \frac{\partial x_3}{\partial \eta_1} = x_{16}, \quad \frac{\partial x_3}{\partial \eta_2} = x_{17}, \quad \frac{\partial x_3}{\partial \eta_3} = x_{18}, \quad \frac{\partial x_3}{\partial \eta_4} = x_{19}, \quad \frac{\partial x_3}{\partial \eta_5} = x_{20}, \\ \frac{\partial x_4}{\partial \eta_1} = x_{21}, \quad \frac{\partial x_4}{\partial \eta_2} = x_{22}, \quad \frac{\partial x_4}{\partial \eta_3} = x_{23}, \quad \frac{\partial x_4}{\partial \eta_4} = x_{24}, \quad \frac{\partial x_4}{\partial \eta_5} = x_{25}, \\ \frac{\partial x_5}{\partial \eta_1} = x_{26}, \quad \frac{\partial x_5}{\partial \eta_2} = x_{27}, \quad \frac{\partial x_5}{\partial \eta_3} = x_{28}, \quad \frac{\partial x_5}{\partial \eta_4} = x_{29}, \quad \frac{\partial x_5}{\partial \eta_5} = x_{30}. \end{aligned}$$

The shooting technique requires simultaneously integrating Eqs. (55)–(59) in addition to time derivatives of above terms (for a total of 30 first order differential equations) for one period of excitation.

The initial conditions are defined as

$$\begin{aligned} x_1(0) = \eta_1, \quad x_2(0) = \eta_2, \quad x_3(0) = \eta_3, \quad x_4(0) = \eta_4, \quad x_5(0) = \eta_5, \\ x_6(0) = 1, \quad x_7(0) = 0, \quad x_8(0) = 0, \quad x_9(0) = 0, \quad x_{10}(0) = 0, \\ x_{11}(0) = 0, \quad x_{12}(0) = 1, \quad x_{13}(0) = 0, \quad x_{14}(0) = 0, \quad x_{15}(0) = 0, \\ x_{16}(0) = 0, \quad x_{17}(0) = 0, \quad x_{18}(0) = 1, \quad x_{19}(0) = 0, \quad x_{20}(0) = 0, \\ x_{21}(0) = 0, \quad x_{22}(0) = 0, \quad x_{23}(0) = 0, \quad x_{24}(0) = 1, \quad x_{25}(0) = 0, \\ x_{26}(0) = 0, \quad x_{27}(0) = 0, \quad x_{28}(0) = 0, \quad x_{29}(0) = 0, \quad x_{30}(0) = 1. \end{aligned}$$

The thirty first order differential equations are then integrated numerically subjected to the initial conditions over the duration of one period T . Subsequently, we calculate $x_6 - x_{30}$ at time T and substitute them in the below algebraic system of equations and solve for the error in the initial conditions:

$$\begin{bmatrix} x_6 - 1 & x_7 & x_8 & x_9 & x_{10} \\ x_{11} & x_{12} - 1 & x_{13} & x_{14} & x_{15} \\ x_{16} & x_{17} & x_{18} - 1 & x_{19} & x_{20} \\ x_{21} & x_{22} & x_{23} & x_{24} - 1 & x_{25} \\ x_{26} & x_{27} & x_{28} & x_{29} & x_{30} - 1 \end{bmatrix} \begin{bmatrix} \partial \eta_1 \\ \partial \eta_2 \\ \partial \eta_3 \\ \partial \eta_4 \\ \partial \eta_5 \end{bmatrix} = \begin{bmatrix} \eta_{10} - x_1 \\ \eta_{20} - x_2 \\ \eta_{30} - x_3 \\ \eta_{40} - x_4 \\ \eta_{50} - x_5 \end{bmatrix}$$

The procedure is repeated until the errors are minimized and a convergence is achieved. Figs. 10 and 11 reveal the stable numerical solutions compared with analytical solutions for the cantilever beam response and output voltage, respectively. Both long time integration (LTI) and shooting methods are applied to get numerical solutions of the frequency responses. Analytical solutions near the central frequency in the frequency spectrum indicate unstable solutions, which cannot be obtained from long time integration. Solutions by LTI match with those of the shooting method very well. It is observed that there is an agreement between analytical and numerical solutions on having two branches tilted to both sides; however, there is a quantitative difference between analytical solutions and numerical solutions. The maximum errors between the numerical and analytical solutions are 25% on the left branch and 34% on the right branch, respectively. The difference between analytical solutions and numerical solutions in the large amplitude range comes from the assumption of only linear terms for asymptotic series solutions for $S(t)$, $\alpha(t)$ and $\nu(t)$ (Eqs. (32)). In addition, the second and higher order terms of time derivatives are also dropped. If higher order terms were added to the assumed solutions, more accurate solutions would have been obtained by the multiple scales method, but adding more terms makes the derivations computationally very sophisticated. Regardless of small differences, all methods indicate the double bending of frequency response and broadening of the frequency bandwidth.

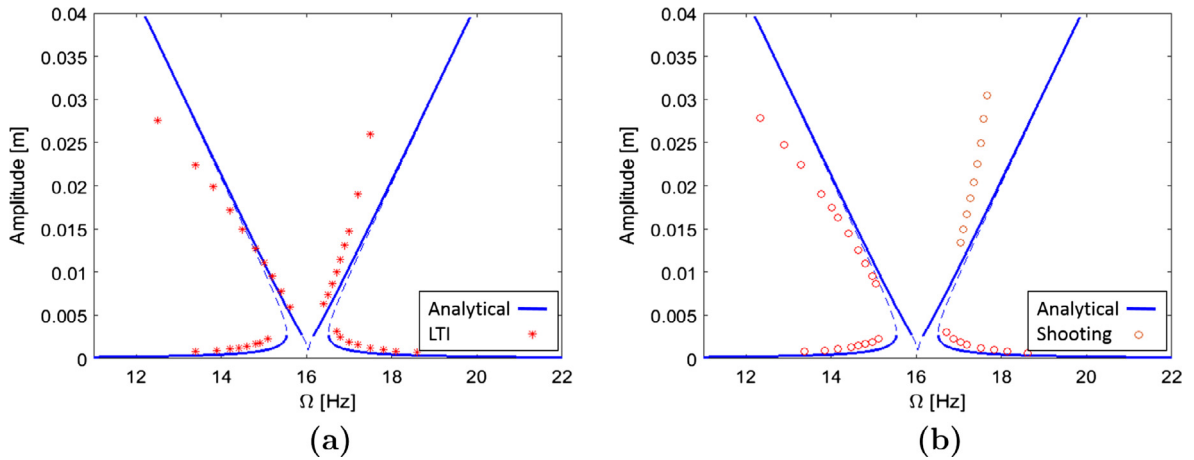


Fig. 10. (a) Cantilever beam frequency response by long time integration (LTI), (b) cantilever beam frequency response by shooting.

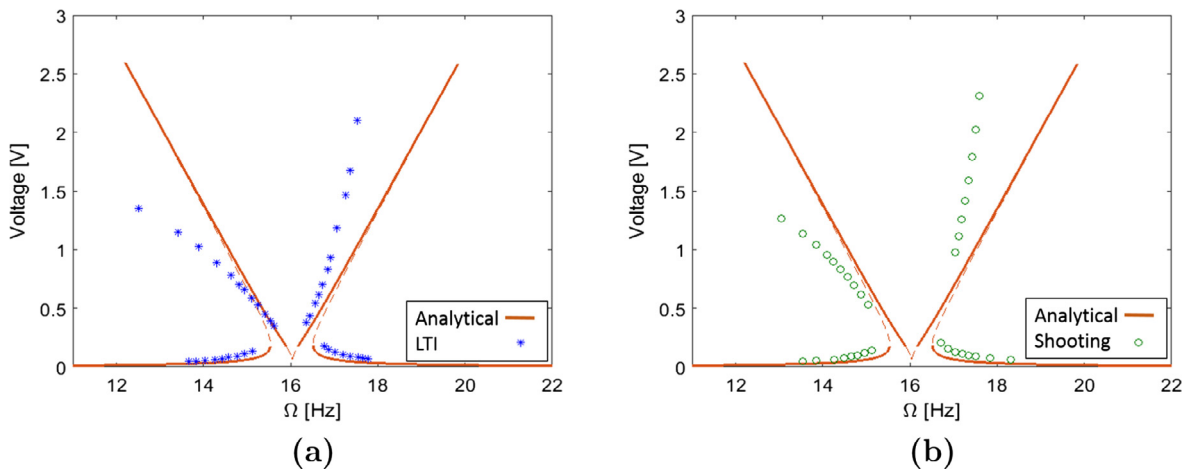


Fig. 11. (a) Output voltage frequency response by long time integration, (b) output voltage frequency response by shooting.

5. Conclusions

In this paper, the dynamic behavior of a hybrid resonator that combines internal resonance with bi-stability is explored to increase frequency bandwidth. The hybrid resonator consists of a piezoelectric cantilever beam carrying a movable magnet facing a fixed magnet. The two magnets face one another with the same pole to create a bi-stable system, while internal resonance is made by adding a spring that controls the movable magnet.

Three coupled governing equations are obtained by using Hamilton's energy approach. The perturbation method of multiple scales is employed to obtain approximate analytical solutions for the amplitude and voltage frequency responses. The amplitude and voltage frequency responses reveal a double bending effect, two frequency peaks bending to opposite sides of the central frequency, resulting in a broader frequency bandwidth. Compared to bi-stable energy harvesters with two fixed magnets that have only one branch, the bandwidth of the new design is two times larger. The effects of different system parameters on the frequency response and output voltage curves are studied. It is concluded that the larger the magnetization moment and the smaller the initial distance between magnets, the larger the frequency bandwidth. Variation of spring stiffness changed the symmetry of the frequency response and shifted the central frequency, but a large amplitude response was maintained. The approximate analytical solutions are also verified by the numerical methods of long time integration (Runge-Kutta method) and the shooting technique for a case study. Analytical and numerical solutions are in good agreement. In summary, the hybrid energy harvester improves energy conversion efficiency by extending the frequency bandwidth of response and voltage combining the two effects of bi-stability and internal resonance.

Appendix A. Supplementary material

Supplementary data associated with this article can be found, in the online version, at <http://dx.doi.org/10.1016/j.ymssp.2016.12.032>.

References

- [1] S.P. Pellegrini, N. Tolou, M. Schenk, J.L. Herder, Bistable vibration energy harvesters: a review, *J. Intell. Mater. Syst. Struct.* (2012), p. 1045389X12444940.
- [2] M.F. Daqaq, R. Masana, A. Erturk, D.D. Quinn, On the role of nonlinearities in vibratory energy harvesting: a critical review and discussion, *Appl. Mech. Rev.* 66 (4) (2014) 040801.
- [3] H. Liu, Y. Qian, N. Wang, C. Lee, An in-plane approximated nonlinear MEMS electromagnetic energy harvester, *J. Microelectromech. Syst.* 23 (3) (2014) 740–749.
- [4] H. Liu, C.J. Tay, C. Quan, T. Kobayashi, C. Lee, Piezoelectric MEMS energy harvester for low-frequency vibrations with wideband operation range and steadily increased output power, *J. Microelectromech. Syst.* 20 (5) (2011) 1131–1142.
- [5] L. Dhakar, H. Liu, F. Tay, C. Lee, A new energy harvester design for high power output at low frequencies, *Sens. Actuat. A: Phys.* 199 (2013) 344–352.
- [6] R. Masana, M.F. Daqaq, Relative performance of a vibratory energy harvester in mono- and bi-stable potentials, *J. Sound Vib.* 330 (24) (2011) 6036–6052.
- [7] R. Masana, M.F. Daqaq, Electromechanical modeling and nonlinear analysis of axially loaded energy harvesters, *J. Vib. Acoust.* 133 (1) (2011) 011007.
- [8] T. Yildirim, M.H. Ghayesh, W. Li, G. Alici, Design and development of a parametrically excited nonlinear energy harvester, *Energy Convers. Manage.* 126 (2016) 247–255.
- [9] F. Cottone, H. Vocca, L. Gammaitoni, Nonlinear energy harvesting, *Phys. Rev. Lett.* 102 (8) (2009) 080601.
- [10] B. Mann, B. Owens, Investigations of a nonlinear energy harvester with a bistable potential well, *J. Sound Vib.* 329 (9) (2010) 1215–1226.
- [11] S.C. Stanton, C.C. McGehee, B.P. Mann, Nonlinear dynamics for broadband energy harvesting: investigation of a bistable piezoelectric inertial generator, *Physica D* 239 (10) (2010) 640–653.
- [12] B. Ando, S. Baglio, C. Trigona, N. Dumas, L. Latorre, P. Nouet, Nonlinear mechanism in MEMS devices for energy harvesting applications, *J. Micromech. Microeng.* 20 (12) (2010) 125020.
- [13] M. Ferrari, V. Ferrari, M. Guizzetti, B. Andò, S. Baglio, C. Trigona, Improved energy harvesting from wideband vibrations by nonlinear piezoelectric converters, *Sens. Actuat. A: Phys.* 162 (2) (2010) 425–431.
- [14] H. Vocca, I. Neri, F. Travasso, L. Gammaitoni, Kinetic energy harvesting with bistable oscillators, *Appl. Energy* 97 (2012) 771–776.
- [15] L. Tang, Y. Yang, C.-K. Soh, Improving functionality of vibration energy harvesters using magnets, *J. Intell. Mater. Syst. Struct.* (2012), p. 1045389X12443016.
- [16] L. Tang, Y. Yang, C.K. Soh, Toward broadband vibration-based energy harvesting, *J. Intell. Mater. Syst. Struct.* 21 (18) (2010) 1867–1897.
- [17] B. Mann, N. Sims, Energy harvesting from the nonlinear oscillations of magnetic levitation, *J. Sound Vib.* 319 (1) (2009) 515–530.
- [18] Y. Chen, T.E. Pollock, A. Salehian, Analysis of compliance effects on power generation of a nonlinear electromagnetic energy harvesting unit; theory and experiment, *Smart Mater. Struct.* 22 (9) (2013) 094027.
- [19] D.A. Barton, S.G. Burrow, L.R. Clare, Energy harvesting from vibrations with a nonlinear oscillator, *J. Vib. Acoust.* 132 (2) (2010) 021009.
- [20] G. Sebald, H. Kuwano, D. Guyomar, B. Ducharne, Experimental duffing oscillator for broadband piezoelectric energy harvesting, *Smart Mater. Struct.* 20 (10) (2011) 102001.
- [21] S. Shahruz, Increasing the efficiency of energy scavengers by magnets, *J. Comput. Nonlinear Dyn.* 3 (4) (2008) 041001.
- [22] S.P. Beeby, R. Torah, M. Tudor, P. Glynn-Jones, T. O'Donnell, C. Saha, S. Roy, A micro electromagnetic generator for vibration energy harvesting, *J. Micromech. Microeng.* 17 (7) (2007) 1257.
- [23] M.F. Daqaq, Response of uni-modal duffing-type harvesters to random forced excitations, *J. Sound Vib.* 329 (18) (2010) 3621–3631.
- [24] M.A. Karami, D.J. Inman, Equivalent damping and frequency change for linear and nonlinear hybrid vibrational energy harvesting systems, *J. Sound Vib.* 330 (23) (2011) 5583–5597.
- [25] H.-X. Zou, W.-M. Zhang, K.-X. Wei, W.-B. Li, Z.-K. Peng, G. Meng, A compressive-mode wideband vibration energy harvester using a combination of bistable and flexensional mechanisms, *J. Appl. Mech.* 83 (12) (2016) 121005.
- [26] H. Wu, L. Tang, Y. Yang, C.K. Soh, Development of a broadband nonlinear two-degree-of-freedom piezoelectric energy harvester, *J. Intell. Mater. Syst. Struct.* 25 (14) (2014) 1875–1889.
- [27] L. Tang, Y. Yang, A nonlinear piezoelectric energy harvester with magnetic oscillator, *Appl. Phys. Lett.* 101 (9) (2012) 094102.
- [28] B. Andò, S. Baglio, F. Maiorca, C. Trigona, Analysis of two dimensional, wide-band, bistable vibration energy harvester, *Sens. Actuat. A: Phys.* 202 (2013) 176–182.
- [29] I. Sari, T. Balkan, H. Kulah, An electromagnetic micro power generator for wideband environmental vibrations, *Sens. Actuat. A: Phys.* 145 (2008) 405–413.
- [30] A. Nayfeh, D. Mook, *Nonlinear Oscillations*, Wiley, New York, 1979.
- [31] C. Lan, W. Qin, W. Deng, Energy harvesting by dynamic instability and internal resonance for piezoelectric beam, *Appl. Phys. Lett.* 107 (9) (2015) 093902.
- [32] L.-Q. Chen, W.-A. Jiang, Internal resonance energy harvesting, *J. Appl. Mech.* 82 (3) (2015) 031004.
- [33] D. Cao, S. Leadenham, A. Erturk, Internal resonance for nonlinear vibration energy harvesting, *Eur. Phys. J. Special Top.* 224 (14–15) (2015) 2867–2880.
- [34] L.-Q. Chen, W.-A. Jiang, M. Panyam, M.F. Daqaq, A broadband internally resonant vibratory energy harvester, *J. Vib. Acoust.* 138 (6) (2016) 061007.
- [35] L. Xiong, L. Tang, B.R. Mace, Internal resonance with commensurability induced by an auxiliary oscillator for broadband energy harvesting, *Appl. Phys. Lett.* 108 (20) (2016) 203901.
- [36] W. Yang, S. Towfighian, Nonlinear vibration energy harvesting based on variable double well potential function, in: *Proc. of SPIE, Active and Passive Smart Structures and Integrated Systems*, vol. 9799, 2016, pp. 979902-1–979902-10.
- [37] S.A. Siddiqui, M.F. Golnaraghi, G.R. Heppler, Dynamics of a flexible cantilever beam carrying a moving mass, *Nonlinear Dyn.* 15 (2) (1998) 137–154.
- [38] G. Michaltsos, D. Sophianopoulos, A. Kounadis, The effect of a moving mass and other parameters on the dynamic response of a simply supported beam, *J. Sound Vib.* 191 (3) (1996) 357–362.
- [39] G. Michaltsos, Dynamic behaviour of a single-span beam subjected to loads moving with variable speeds, *J. Sound Vib.* 258 (2) (2002) 359–372.
- [40] Y. Jia, A.A. Seshia, An auto-parametrically excited vibration energy harvester, *Sens. Actuat. A: Phys.* 220 (2014) 69–75.
- [41] M.I. Younis, *MEMS Linear and Nonlinear Statics and Dynamics*, vol. 20, Springer Science & Business Media, 2011.